Lubrication Forces between Surfaces Bearing Polymer Brushes

Jacob Klein,*,†,‡ Yoichiro Kamiyama,†,⊥ Hisae Yoshizawa,† Jacob N. Israelachvili,†,§ Glenn H. Fredrickson,§ Philip Pincus,† and Lewis J. Fetters‖

Materials and Interfaces Department, Weizmann Institute, Rehovot 76100, Israel, Materials Department and Department of Chemical and Nuclear Engineering, University of California at Santa Barbara, California 93106, and Exxon Research and Engineering Company, Clinton Township, New Jersey 08801

Received February 19, 1993; Revised Manuscript Received May 19, 1993⊗

ABSTRACT: We have studied both the equilibrium and the hydrodynamic lubrication forces that act in the normal direction between mica surfaces in toluene when bearing polystyrene chains anchored to each surface by a zwitterionic group at one end. The quasistatic force–distance profiles reveal the long-ranged repulsion characteristic of steric interactions between the extended brush-like layers in the good solvent and provide a measure of the brush thickness L in close agreement with earlier studies of such brushes. Dynamic measurements of the surface forces, where the surface separation D is varied sinusoidally in time, show two regimes: at $D > 2.5L$, the hydrodynamic forces are characteristic of Newtonian flow of liquid with the viscosity of bulk toluene, but with a shear plane shifted a distance L_H from each mica surface (qualitatively similar to earlier observations with adsorbed homopolymer layers). We find that $L \approx L_H$. When the layers are compressed ($D < 2L$), the hydrodynamic forces are dominated by flow of solvent through the confined polymer layers in the gap. They may be described by an "effective viscosity" which increases as D decreases, varying in fair quantitative accord with a recent model. At the highest compressions ($D < L/2$) the confined polymer layers behave in a solid-like manner, suggesting that the confinement between the surfaces greatly increases molecular relaxation times.

I. Introduction

Adsorbed or grafted polymers are commonly used to stabilize colloidal dispersions in a variety of systems, ranging from pharmaceuticals to ferrofluids.[1,2] In recent years the nature of the interactions between polymer-bearing surfaces has been widely studied, both theoretically[3-6] and by direct measurements.[7,8] In particular, extensive use of the mica surface force balance has enabled determination of the quasi-equilibrium force distance laws between surfaces bearing both adsorbed and grafted polymers in a broad range of conditions.[7] Such experiments are sufficiently direct to allow detailed comparison with microscopic models, and the physics of these equilibrium forces is now reasonably well understood.[3-8] Much less is known about the forces that act between polymer-bearing surfaces when they are in relative motion.[9,10] These are important in determining the rheological behavior of sterically-stabilized dispersions, especially at high concentrations of the diperse phase,[11] where hydrodynamic interactions may dominate the equilibrium forces. Such interactions, associated with the flow of liquid between solid surfaces in relative motion, are known as lubrication forces.[12] They play a central role in a range of applications, most obviously in effects involving sliding and friction (and its reduction) between solids,[13] but also in the flow of fluids past surfaces,[14] the rheological properties of multiphase systems,[11] and the flocculation and aggregation rates of colloidal solutions.[15]

The problem of hydrodynamic forces between smooth solid surfaces moving with respect to each other in a liquid is classical.[12] For the case of two flat parallel surfaces a distance D apart moving parallel to each other at relative velocity v, the shear stress is given by

$$\sigma = \dot{\gamma}\eta \tag{1}$$

where $\dot{\gamma} = v/D$ is the shear rate, and η the shear viscosity of the fluid. The case of a sphere moving parallel (and close) to a flat surface is more complicated and has been analyzed only recently.[12,16] The geometry of the experiments described in this paper is that of a sphere, radius R, moving at velocity $dD/dt = \dot{D}$ normally with respect to a flat surface a closest distance D apart. In the lubrication limit $R \gg D$ Reynolds[17] showed in 1886 that, for a Newtonian liquid of shear viscosity η, a hydrodynamic force F_H, given by

$$F_H = 6\pi R^2 \eta(\dot{D}/D) \tag{2}$$

acts to oppose the motion. This force is due to a transverse pressure gradient in the annular region between the surfaces, which causes the viscous liquid to flow radially out of (or into) the gap as the surfaces approach (or recede).

In the present work we are mainly concerned with lubrication forces between surfaces bearing polymers in a liquid medium. In such cases, where layers of surface-attached chains are trapped and compressed, as indicated in Figure 1, flow of the liquid within the intersurface gap is further impeded by the need for it to pass through the network-like polymer structure. The result can be a large magnification of the lubrication force F_H. This effect was noted already during early measurements of forces between mica surfaces bearing adsorbed polystyrene in cyclohexane in poor solvent conditions.[18,19] An analysis[18] based on a simplified extension of eq 2 indicated a strong enhancement (by a factor of order 100) of the time it would take for the two polymer-bearing surfaces to jump into contact under an attractive force, relative to the time expected for such a jump in the absence of polymer; such enhancement of jump times was indeed observed experimentally.[18,19]

In recent years the mica surface force apparatus, used originally for the direct measurement of the *quasi-equilibrium* interactions $F(D)$ between curved mica sur-

† Materials Department, UCSB.
‡ Permanent and correspondence address: Weizmann Institute.
§ Chemical and Nuclear Engineering, UCSB.
⊥ On leave from Fuji Photo Film Co. Ltd. (Japan).
‖ Exxon.
⊗ Abstract published in *Advance ACS Abstracts*, August 15, 1993.

0024-9297/93/2226-5552$04.00/0

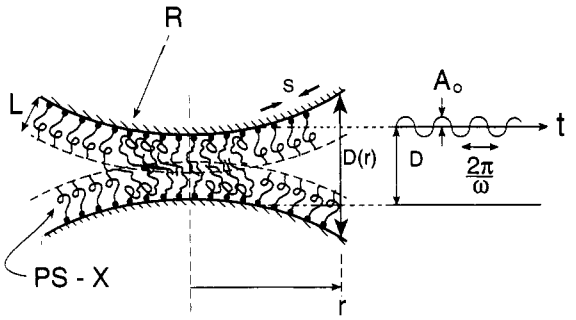

Figure 1. Schematic illustration of curved interacting surfaces (radius of curvature R) bearing polystyrene chains attached by one end (via the zwitterion X at that end) with a mean interanchor spacing s and a brush thickness L. In the dynamic experiments the top surface is moved sinusoidally with amplitude A_0, so that the distance of closest approach D varies as $(D + A\sin(\omega t))$. $D(r)$ is the surface separation at a radial distance r as shown.

faces a closest distance D apart,[18,20] has been extended also to the systematic study of friction and *lubrication* forces between such surfaces.[21-25] In these, the forces are measured while the mica surfaces are in relative normal or lateral motion. Studies have been carried out in simple liquids,[21-23] in polymer melts,[24-26] and in the presence of adsorbed polymers[10,27,28] and surfactant layers.[29] Two main approaches have been employed for the case of normal relative motion of the mica surfaces. In the first, Chan and Horn[21] applied a constant motion to the base of the spring supporting one of the surfaces, driving it toward the other; from the change in the resulting separation D between the surfaces, the force F_H was obtained as a function of time. By applying Reynolds' equation together with the appropriate (equilibrium) intersurface force $F(D)$—determined separately in the usual quasistatic method—they were able to show that the measured rate of approach of the surfaces across the thin liquid films was as expected theoretically, if the viscosity of the liquid equals its bulk Newtonian value down to a few nanometers. Horn and Israelachvili subsequently showed this was true also for a much more viscous oligomeric liquid.[30]

In the other approach Israelachvili,[22] and subsequently Montfort and Hadziioannou,[25] applied a sinusoidal motion to one of the surfaces so that the separation D between them also varied sinusoidally. For a motion $A_0\sin(\omega t)$ applied to the top surface, and as long as the driving frequency ω is much lower than the resonant frequency of the supporting spring, the separation between the surfaces varies as

$$D'(t) = D + A\sin(\omega t + \phi) \tag{3}$$

and the following relation holds:

$$6\pi R^2\omega/(K[(A_0/A)^2 - 1]^{1/2}) \equiv \mathcal{G}(R,\omega,A_0,K) = D/\eta_0 \tag{4}$$

where R is the mean radius of curvature of the two mica sheets, K is the constant of the spring supporting the lower mica surface in the surface-force apparatus, and η_0 is the viscosity of the medium separating the surfaces.[31] The left-hand side of eq 4, designated $\mathcal{G}$, is a central quantity in the present work. From eq 2 we may write $\mathcal{G} = 6\pi R^2(\dot{D}/F_H)$; i.e., it is proportional to the mutual velocity $\dot{D}$ of the surfaces per unit instantaneous hydrodynamic force F_H. In this sense $\mathcal{G}$ may be thought of as an "effective mobility" of the top surface as it moves with respect to the lower one. Larger $\mathcal{G}$ values imply that it is easier to push the surfaces together (or apart). From eq 4 a plot of $\mathcal{G}$ against surface separation D should yield a straight line with slope $(1/\eta_0)$ running through the origin ($D = 0$). For the case where each surface bears a polymer layer of some effective hydrodynamic thickness L_H, eq 4 still holds for $D \gg 2L_H$, but the equation is now modified to[27]

$$\mathcal{G} = (D - 2L_H)/\eta_0 \tag{5}$$

This is equivalent to shifting the plane of shear (defining the no-slip boundary) in the original Reynolds equation from the original (polymer-free) solid–liquid interfaces to a distance L_H from each surface. A plot of eq 5 should then manifest a linear regime at $D \gg 2L_H$, with a slope η_0^{-1} and an intercept $D = 2L_H$. In a study of polystyrene adsorbed onto mica from cyclohexane at room temperature[27] (poor solvent conditions), precisely such behavior was observed (with $L_H \approx R_g$, the polymer radius of gyration). At $D \leq 2L$, however, where L is the actual thickness of each brush, the polymer layers come into overlap (Figure 1), solvent must flow within the layers as the surfaces approach or recede, and the behavior becomes more complicated. Such behavior has not, to date, been experimentally investigated.

Recently, two of us have analyzed[32] the form of the lubrication forces expected between two polymer-bearing surfaces in mutual normal motion at separations much less than twice the hydrodynamic thickness of the layers (i.e., under strong compression). The precise behavior is sensitive to the way in which the hydrodynamic screening length depends on the segment concentrations within the surface-attached polymer layer, as will be discussed in more detail later. From this analysis it is possible to deduce the form of the lubrication forces at $D \ll 2L$ and to recast the right-hand side of eq 4 in a way which accounts for the additional forces acting on the fluid as it is forced through the polymer network compressed between the surfaces.

The experiments described in this paper were designed to examine the lubrication interactions between two surfaces bearing end-attached (but otherwise nonadsorbing) polymers in a good solvent (polystyrene in toluene) over the entire range $2L \ll D \ll 2L$ and in addition to compare the results critically with the above theoretical model. In section II we describe the experimental methods and the materials used, and in section III we present the results. In section IV the theoretical model is discussed and compared with the data in the appropriate surface-separation regime. We conclude with some remarks on the dynamics and the stability of confined polymer layers and on the relation of the present study to the case of lubrication forces between polymer-bearing surfaces undergoing pure shear motion.[10,28]

II. Experimental Section

Apparatus. The experiments were carried out using a mica surface force balance[18,20] (MkIII). In this, curved mica sheets are mounted opposite each other in a crossed cylinder configuration. The separation of closest approach D between the surfaces (which are half-silvered on their back surface) is measured via optical interferometry to within ±3 Å in the range from contact ($D = 0$) to a few thousand angstroms. The shape of the interferometric fringes gives the mean radius of curvature R (≈1 cm) of the mica sheets. The separation D is controlled via a multistage mechanism. The fine stage is a piezoelectric tube (PZT) on which the top mica surface is mounted and which can move it normally (by axial contraction or expansion of the PZT in response to an applied voltage) with respect to the lower mica surface. This lower surface is mounted on a rigid support via a flexible leaf of spring constant K, whose bending yields the normal force between the surfaces. The spring stiffness can be varied from the outside of the apparatus during the course of an experiment within the range of values $K \approx 10^2$–10^3 N/m. For the dynamic measurements the interferometric fringe pattern is recorded on a video casette recorder (VCR), and the variation of D—as the top surface is moved sinusoidally via a periodic potential applied to the PZT—is

Table I[a]

polymer	M_w	M_w/M_n	R_g (Å)	R_F (Å)
PS	1.31×10^5	1.03	89	315
PS-X(375K)	3.75×10^5	1.03	173	575

[a] The polystyrenes were synthesized and (in the case of the PS-X) end-functionalized as described earlier.[33] Molecular weights were determined by size exclusion chromatography and by light scattering. R_g and R_F are the values of the unperturbed radii of gyration and of the rms swollen end-to-end dimension of the polymers in toluene.[33] The zwitterionic group (designated X) has the structure $[N^+(CH_3)_2(CH_2)_3SO_3^-]$.

analyzed from the video recording subsequent to the experimental runs.[22] In these experiments the amplitude of the sinusoidal motion and its frequency (A_0 and $(\omega/2\pi)$ in eq 3) were varied in the range 500–3000 Å and 0.1–1 Hz, respectively. The room temperature of the experiments was 22.5 ± 0.5 °C throughout.

Materials. All solvents used were analytical grade and used as received. The sucrose (used as glue) was analytical grade (BDH). The polymers used were an unfunctionalized polystyrene (designated PS), which was used for control measurements, and polystyrene terminated with the zwitterionic group $[N^+(CH_3)_2(CH_2)_3SO_3^-]$ (designated PS-X(375K)), which was used to create the end-attached polymer layer. Their molecular characteristics and provenance are given in Table I. Identical polymers were previously used as part of an extensive study[33] of the structure of surface-attached polymer brushes and their mutual interactions.

Procedure. The experimental procedure was as follows: the apparatus and the cylindrical glass lenses on which the mica sheets were to be mounted were cleaned by sonication in toluene, rinsed with filtered ethanol, and allowed to dry in a laminar flow hood. The mica sheets were glued onto the lenses using sucrose as glue (melting grains of sucrose on the lenses, laying a mica sheet on each lens, and allowing to cool) and were then mounted into the apparatus. After determining the air contact wavelengths of the interference fringes, toluene was introduced and the force–separation profile $F(D)$ was determined in the usual (quasistatic) way, using a differential approach to minimize the effects of thermal drift.[34] Dynamic measurements in the polymer-free toluene were then carried out. The unfunctionalized polymer PS was then added to the required concentration, and $F(D)$ was determined after a suitable incubation period to verify that no adsorption of the unfunctionalized chains was occurring in the conditions of the experiments. Following this, dynamic measurements were again performed as a control. Finally, the zwitterion-terminated PS-X(375K) was added to the cell. After incubation in the solution and formation of the end-attached polystyrene brush, normal force profiles $F(D)$ and dynamic force measurements were carried out. For the dynamic measurements, the driving amplitude A_0, frequency ω, and spring constant K were also varied at each position so as to optimize the value of A at the different surface separations.[35]

III. Results

Normal force profiles $F(D)$ in the quasistatic mode and the "viscosity profiles" (eq 4) in the dynamic mode were first determined in the polymer-free solvent. The force–distance profile is shown in Figure 2 (circles and squares) and resembles earlier observations[33,36,37] (indicated by the shaded band): little interaction from large separations down to $D \approx 100$ Å, followed by a jump into a strong adhesive contact (to a separation $D \approx 10$ Å relative to the air–contact separation), due to capillary condensation of water between the mica surfaces from the undried toluene. Dynamic measurements ($A_0 = 480$ Å at 1 Hz) in the pure solvent were then carried out.[38] In Figure 3 $\mathcal{G}$ (eq 4) is plotted against the mean surface separation D: this reveals a linear variation whose inverse slope is 0.55 ± 0.02 cP and which intercepts the surface separation (D) axis at $D = 3$ ± 2 nm. This value of the inverse slope is close to the literature value[39] of the viscosity of bulk toluene, $\eta_0 = 0.56$ cP at 23 °C. The intercept on the surface separation axis

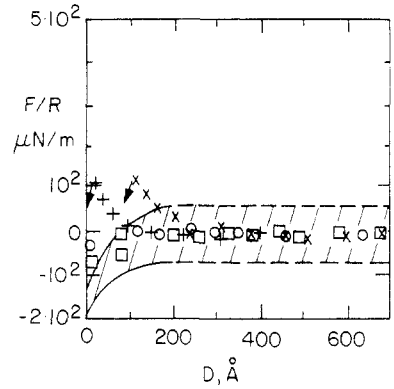

Figure 2. Quasistatic force (F) vs distance (D) profiles between the curved mica surfaces in pure toluene (○, ◇) and following overnight incubation in a 10^{-4} g/mL solution of PS (+, ×). The force profiles are normalized by the mean radius of curvature R ($R = (R_1R_2)^{1/2} \approx 1$ cm, where R_1 and R_2 are the respective radii of the mica surfaces) to yield the interaction energy per unit area in the Derjaguin approximation.[18,20] The shaded band indicates the range of values determined in earlier force–distance profiles in this system.[33,36] Following incubation in the PS solution the surfaces experience a weak short-range repulsion before jumping (arrows) into strong adhesive contact as in the polymer-free solvent.

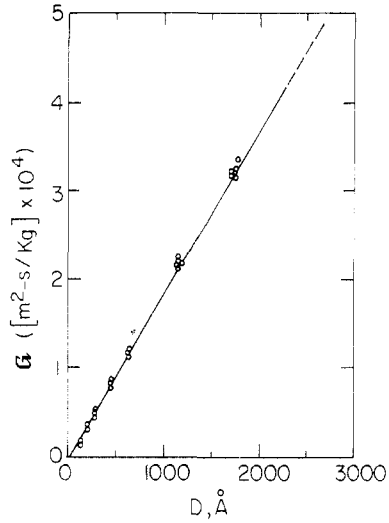

Figure 3. Variation of $\mathcal{G}$ ($\equiv 6\pi R^2\omega/(K[(A_0/A)^2 - 1]^{1/2})$) with surface separation D for curved mica sheets in pure toluene. A frequency of $\omega/2\pi = 1$ Hz and a driving amplitude $A_0 = 480$ Å were used, with $K = 1.44 \times 10^2$ N/m. The straight line has a slope $1/\eta$, with $\eta = 0.55$ cP.

suggests the shear plane is at 1.5 ± 1 nm away from the mica surfaces defined by the air–contact position, possibly due to a thin layer of water adhered strongly to each surface from the toluene.

Following the dynamic measurements in the pure solvent, unfunctionalized polystyrene (PS) was added to the toluene in the cell to a concentration 10^{-4} (±5%) g/mL and the solution stirred. After overnight incubation in the PS solution, the normal force–separation profile was determined: the results are shown in Figure 2 (crosses) and are similar to the F(D) variation in the polymer-free solvent. This is again consistent with the earlier studies[33,36,37] and confirms that there is no significant adsorption of the unfunctionalized polystyrene from the toluene onto the mica.[40] Dynamic measurements were then carried out, and a plot of $\mathcal{G}$ vs D (eq 4), shown in Figure 4, again reveals a linear variation similar to that obtained in the absence of polymer: the inverse slope is 0.54 ± 0.02 cP, while the intercept on the surface separation axis is slightly larger at $D = 10$ ± 3 nm.[41]

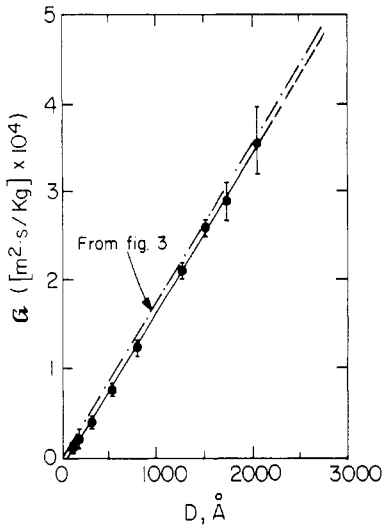

Figure 4. Variation of $\mathcal{G}$ vs D following overnight incubation in 10^{-4} g/mL PS solution in toluene. Values of ω, A_0, and K are as in Figure 3. The straight line has a slope $1/\eta$, with η = 0.54 cP. The broken line is from the fit in Figure 3.

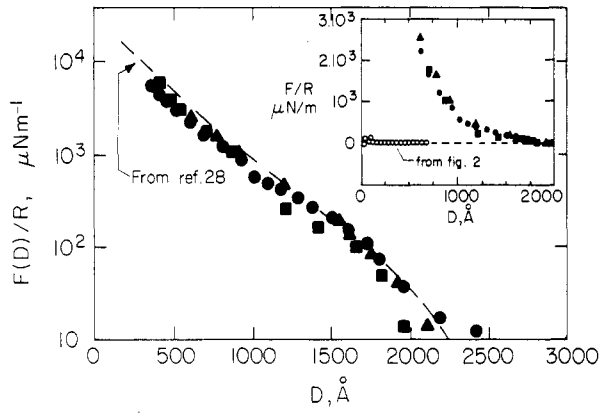

Figure 5. Quasistatic force (F) vs surface separation (D) profiles between curved mica surfaces following overnight (and longer) incubation in 10^{-4} g/mL PS-X solution in toluene (normalized by the mean radii of curvature R of the mica surfaces as explained in the caption to Figure 2). Different symbols refer to different contact positions. The broken curve is taken from force profiles with the identical system from the study by Taunton et al.[33] The inset shows the data on a linear scale, incorporating the data from Figure 2 in the absence of a polymer brush on the surfaces.

Following these controls, the PS-X(375K) was added to the apparatus to a concentration of 10^{-4} (±5%) g/mL, the solution was stirred, and the surfaces were left to incubate overnight. Subsequent measurements of the (quasistatic) force profiles $F(D)$ and of the dynamic profiles $\mathcal{G}$ vs D were carried out at several different points of contact between the interacting mica sheets. The results are summarized in Figures 5 and 6, respectively.

Following incubation in the PS-X(375K) solution, the force–distance profiles (Figure 5) revealed a long-ranged steric interaction due to attachment of the chains to the mica surface. Comparison with the interaction profiles in pure toluene and in the presence of unfunctionalized PS (inset) shows clearly that the attachment of the PS-X(375K) chains is taking place via the zwitterionic end groups to form extended brush-like layers. Repulsive interactions, which commence at D_{onset} = 2250 ± 100 Å, give a measure of the thickness L of each of the brush layers ($L = D_{onset}/2$), while the magnitude of the osmotic repulsion in the highly compressed regime in Figure 5 provides a measure of the adsorbed amount of this polymer on the mica surface. Using the approach described in ref 33, we evaluate this as Γ' = 3 ± 0.5 mg/m^2. This

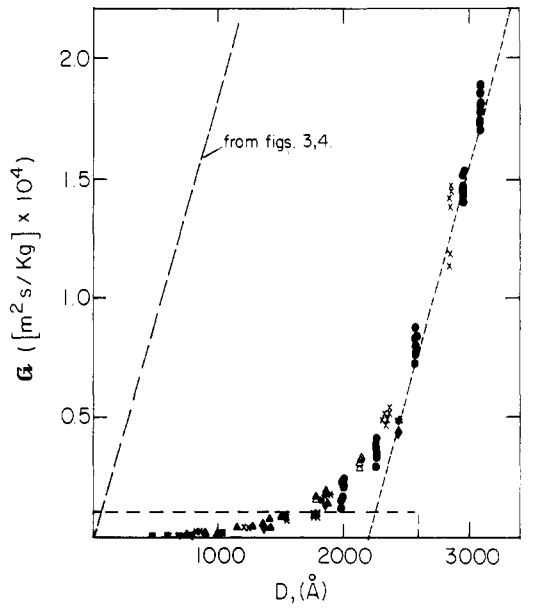

Figure 6. Variation of $\mathcal{G}$ vs D following overnight (and longer) incubation in 10^{-4} g/mL PS-X solution in toluene. Different shaped symbols refer to different contact positions and also to different values of the frequencies and of the amplitudes at which the top mica surface was driven: (×, △, ▲, ▼) $\omega/2\pi$ = 1Hz, A_0 = 480 Å; (●, *) $\omega/2\pi$ = 0.2 Hz, A_0 = 480 Å; (◇) $\omega/2\pi$ = 1 Hz, A_0 = 1440 Å; (□) $\omega/2\pi$ = 1 Hz, A_0 = 2880 Å. Values of the stiffness of the leaf spring supporting the lower mica surface varied from 1.44×10^2 to 1.38×10^3 N/m, with the higher values covering the regions of highest compression (lowest D). The straight line through the data at D > 2500 Å has a slope $1/\eta$, with η = 0.54 cP. The broken line is from Figures 3 and 4 in the absence of a polymer brush.

corresponds to a mean spacing s = 145 ± 15 Å between the zwitterions anchoring the polystyrene chains on the mica substrate (Figure 1), in agreement with the earlier study.[33] Force–distance profiles $F(D)$ were carried out frequently as a control during the course of an experiment; their reproducibility (Figure 5) even after strongly compressive dynamic measurements indicates that the polymer chains do not desorb in the conditions of compression and of fluid flow in this study. In general, the stiffness of the spring constant K was adjusted to lower values (ca. 10^2 N/m) for the $F(D)$ measurements to ensure greater sensitivity in detecting the onset of repulsive interactions and was increased to higher values (ca. 10^3 N/m) for the dynamic measurements to achieve greater accuracy in the regime of high compressions.

Figure 6 shows the results of several dynamic profiles at several different contact positions, where the quantity $\mathcal{G}$ is plotted against mean surface separation D. The plot has a linear region at D > 2500 Å, which is well fitted, as indicated, by a line of inverse slope 0.54 ± 0.02 cP. This is again close to the literature value of the viscosity of bulk toluene. At lower values of the surface separation (D < ca. 2500 Å) the data curve to approach the D axis as shown. The theoretical discussion in the following section—which we will consider in the light of our data—will be concerned with the flow of fluid through surface-attached brushes in the regime where the polymer layers are highly compressed; for this reason we show this regime (corresponding to the broken rectangle in Figure 6) on an expanded scale in Figure 7.

IV. Discussion

To carry out a critical comparison of our results with available theoretical models, it will first be necessary to consider several features of the results presented in the

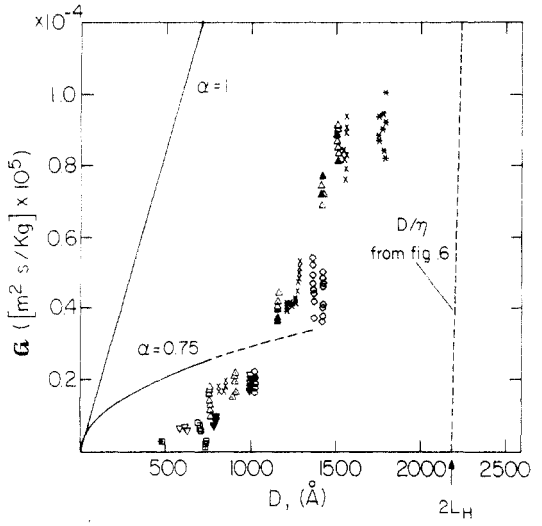

Figure 7. Variation of $\mathcal{G}$ vs D taken from Figure 6, showing the region enclosed in the broken rectangle (Figure 6) on an expanded scale. The two curves are plots of the expression $\mathcal{G} = D/\eta_{eff}$ where η_{eff} = const × $(2/9)\eta_0 a^{-2}\Gamma^{2\alpha}D^{2(1-\alpha)}$ for α = 3/4 and 1, respectively, as indicated. The value used for the solvent viscosity is η_0 = 0.56 cP, the literature value of the viscosity of toluene at 23 °C. The value of the constant prefactor used to calculate the curves is[55] $0.7^{-2} = 2.0$. The straight broken line is from the linear region at D > 2500 Å taken from Figure 6.

previous section. The normal force profiles (Figure 2) and dynamic profiles $\mathcal{G}(D)$ (Figures 3 and 4) in the absence of surface-attached chains are similar to profiles obtained in earlier studies[22,33,36,37] (save that toluene as the liquid medium between the mica sheets has not previously been investigated in the dynamic mode); the $F(D)$ profiles confirm that unfunctionalized polystyrene does not adsorb significantly onto mica from toluene. At the same time, the dynamic profiles indicate an effective viscosity of the toluene in the gap between the surfaces which is close to that of bulk toluene, with a shear plane within a few nanometers of each mica surface.

Following incubation in the PS-X(375K) solution, the normal force profiles revert to the long-ranged repulsion (Figure 5) characteristic of the polymer brushes. These profiles are closely similar to those obtained in earlier studies on the same system, as shown by the broken curve (Figure 5) from the study by Taunton et al.[33] In particular, the effective thickness L of each brush may be estimated as half the distance for onset of repulsion; i.e., $L = D_{onset}/2$ = 1130 ± 50 Å, very close to the value L = 1200 ± 50 Å previously obtained.[33] We note here the stability of the end-attached chains with respect to being forced out of the intersurface gap both in compression and in shear, as indicated by the reproducibility of the $F(D)$ profiles shortly following the dynamic runs. The reasons for this have been considered in detail previously.[10,33,42] Essentially, this stability is the result of the rather large sticking energy (ca. $10k_BT$) of the zwitterionic end group anchoring the chains to each mica surface. It can be shown[42,10] that the force required to disrupt this bond is large when compared with the tension along a chain induced either by the compression of the brushes or by the flow of fluid past them in the dynamic measurements. It is of interest to estimate the shear rates associated with this flow: this rate will depend, among other factors, on the hydrodynamic penetration depth of the fluid into each layer. In the present geometry, the maximum shear rate experienced by the liquid, were it moving between *solid* curved surfaces a closest distance D apart, is given by $\dot{\gamma}_{max} \approx (\dot{D}/D)(R/D)^{1/2}$, occurring at a radial distance $r \approx (RD)^{1/2}$ from the point of closest approach.[21] If the penetration depth of fluid flow into a polymer brush is l_p, then a maximal shear rate of the liquid as the brushes are close to overlap ($D \approx 2L$) may be estimated by the expression for $\dot{\gamma}_{max}$ but replacing D by the penetration depth l_p. The discussion which follows suggests that this penetration depth may at most be only of the order of 100 Å or so in our experiments. Taking $\dot{D} = (\omega/\pi)A_0 \approx 10^3$ Å/s (for A_0 = 480 Å at frequency 1 Hz) and R = 1 cm, this gives (putting l_p = 100 Å in place of D) $\dot{\gamma}_{max} \approx 10^4$ s^{-1}. This is comparable with shear rates encountered in recent studies of the forces between similar brush-bearing surfaces as they slide past each other[10,28] and suggests that—in analogy with the sliding studies, where brush thickening at $\dot{\gamma} \approx 10^4$ s^{-1} was attributed to chain stretching—the fluid at these shear rates may be significantly stretching the chains also in the geometry of the present experiments.

The dynamic profile $\mathcal{G}(D)$ shown in Figure 6 exhibits a linear region $\mathcal{G}(D) \propto D$ at D > 2500 Å; this has an inverse slope which is equal (within the scatter) to the inverse slope in the dynamic profiles in the absence of polymer and is close to the literature value for the viscosity of bulk toluene. Extrapolating this linear regime, we find that it intercepts the surface separation axis at $D = D_H$ = 2200 ± 100 Å (Figure 6). These observations are in line with our earlier discussion (ref 27 and eq 5); in particular, the value of D_H corresponds to an effective shear plane at $L_H = D_H/2$ = 1100 ± 50 Å away from each mica sheet. This is very close to the effective brush layer thickness L = 1130 ± 50 Å derived from the $F(D)$ profiles. This observation runs counter to predictions based on some recent calculations of the velocity profile of liquid flowing past a polymer brush on a planar surface.[43] According to these, the effective shear plane of the liquid is at a depth l_p from the brush surface, due to hydrodynamic penetration of the velocity field into the brush, where $l_p \approx (Ls)^{1/2}$, s being the mean spacing between anchoring chain ends on the substrate surface and L the brush height[44] (Figure 1). Taking s = 145 ± 15 Å and L = 1130 ± 50 Å, we find l_p = 405 ± 50 Å. This corresponds to $L_H = L - l_p$ = 725 ± 60 Å, rather than L_H = 1100 Å ≈ L as is actually observed. The difference is far too large to be attributed to any experimental scatter. Partial reasons for this discrepancy between experiment and theory may include the necessity for some compression of the opposing brushes before onset of repulsion is observed in the normal force ($F(D)$) measurements;[45] this could lead to an effective brush thickness L which may be smaller than the extent of the actual brush, though it is not clear whether the magnitude of this effect would account for the difference. It may also be that the flow field is modifying the form of the segmental density distribution so that assumption of the parabolic form[44,46,47] is no longer valid. Another possibility is that the form of the flow fields as the two curved surfaces approach or recede is not identical with that of a fluid in shear flow past a planar brush, which was the case considered in evaluating the hydrodynamic penetration depth l_p.[43] Whatever the reason, we note that the thickness L of a brush, taken from the quasistatic $F(D)$ profiles as half the surface separation at onset of repulsive interactions, is very close to the hydrodynamic thickness L_H obtained by extrapolating the dynamic profiles $\mathcal{G}(D)$ in accordance with eq 5; this suggests a rather weak penetration of the flow field of the fluid into the brush layer, as anticipated in estimating $\dot{\gamma}_{max}$ above.

Before examining the present results in the light of theory, it is of interest to compare our experiments with the only other study with surface-attached chains in a solvent, which uses the dynamic measurement approach.

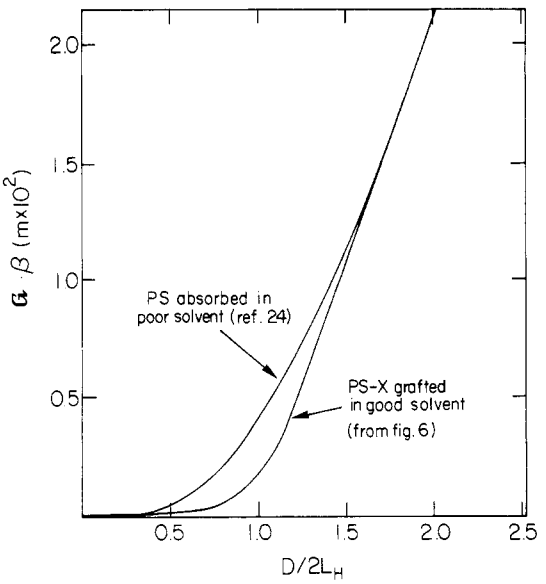

Figure 8. Comparison of the variation of $\mathcal{G}$ with surface separation between mica surfaces bearing adsorbed polystyrene in cyclohexane under poor solvent conditions from ref 27 and between mica surfaces with end-attached polystyrene brushes, taken from Figure 6. The curves are normalized as $D/2L_H$ with respect to the surface separation axis, where $2L_H$ is twice the hydrodynamic thickness of the polymer layers, and as $\mathcal{G} \cdot \eta\beta$ with respect to the $\mathcal{G}$ axis, where $1/\eta$ is the slope of the straight portion of the data and β is the ratio of the hydrodynamic thickness of the respective polymer layers to that of the grafted (PS-X) layer.

In this, "viscosity profiles" $\mathcal{G}$ vs D were obtained between mica sheets bearing adsorbed polystyrene in cyclohexane in poor solvent conditions.[27] The comparison is made in Figure 8, where the surface separation axis is reduced to units of the respective hydrodynamic layer thicknesses L_H. The values of the layer thicknesses differ when cast in terms of the unperturbed radii of gyration R_g of the polymers: $L_H \approx 1\ R_g$ and $6.5\ R_g$ for polystyrene in cyclohexane[27] (poor solvent) and in toluene (good solvent)—from Figure 5—respectively. The larger thickness in the latter case is not surprising in view of both the better solvency state of polystyrene in toluene and the (stretched) brush-like structure of the end-attached chain.[33] The different shapes of the viscosity profiles at $D < 2L_H$ may reflect the rather different segment density profiles expected in the two cases or differences in the way that the hydrodynamic screening length varies with segment concentration at different solvent quality (see later discussion and footnote 56); it may also reflect the fact that the normal force profile is attractive in the poor solvent over much of the regime $D < 2L$ but is monotonically repulsive in the good solvent case. We remark that for the adsorbed chains the value of $L_H \approx 260$ Å $\approx 1\ R_g$ for this polymer, while the effective adsorbed layer thickness for the same polymer, estimated from the distance for onset of (attractive) interactions,[19] is $L \approx 400$ Å. That is, there appears to be a significant penetration of the flowing liquid into the adsorbed layers in the poor solvent case, in contrast to the present study.

The indications above lead us to consider in more detail the question of the lubrication forces in the conditions of our experiments. As noted in the Introduction, the Reynolds lubrication force law given in eq 2 is strictly valid only for the compression (or retraction) of surfaces that confine a Newtonian solvent to a narrow gap of thickness $D \ll R$. When these conditions are met, the solvent velocity field has a dominant radial component that depends parabolically on the gap normal coordinate, z (i.e., normal to the mica surfaces in our experiments). This flow is driven by a radial pressure gradient that is a consequence of the normal motion of the surfaces and the virtual incompressibility of the liquid solvent. The force formula, eq 2, arises from integrating this dynamic pressure field over one of the surfaces.

For the case of surfaces with end-grafted polymers, the hydrodynamics under relative normal motion can be much more complicated than that just described. At separations such that the polymer layers do not interpenetrate, $D > 2L$, the situation is still rather simple, since a Newtonian fluid gap exists between the layers. As evident from our comparison above of the quasistatic force profiles with the dynamic ones, solvent flow only penetrates into the layers a small distance, l_p. Hence, the velocity and pressure fields should be similar to those in the absence of polymer, except that the effective no-slip hydrodynamic boundaries have been moved out from the solid surfaces by a distance $L_H = L - l_p$. It follows,[27] as noted also in section I, that the Reynolds formulas can still be applied, but with D replaced by $(D - 2L_H)$. Because most of the viscous dissipation occurs in the Newtonian gap, a plot of $\mathcal{G}$ vs D should still yield a straight line with the slope $1/\eta_0$. Indeed, Figure 6 is a confirmation of this prediction.

Once the polymer layers interpenetrate, i.e., $D < 2L$, the nature of the hydrodynamic flow is changed. The solvent must avoid the polymer segments, which by virtue of the end-anchoring can undergo no large-scale displacements. Relative motion of polymer and solvent occurs, with the net effect that the solvent experiences a larger frictional drag at a given surface separation D than it would if the polymer were not present. The lubrication flow in this regime of overlapping layers is thus much like the flow of a Newtonian fluid in a porous medium, and this analogy was recently exploited[32] to investigate lubrication forces for overlapped layers. It was assumed that the overlap was sufficient, $D \ll 2L$, to produce a uniform concentration of polymer segments normal to the surfaces, but not so high that the polymer volume fraction ϕ becomes significant (semidilute regime[48]). If the chains are permanently affixed to the surfaces (as is the case in the present experiments, where the surface-attached chains are not extruded from the intersurface gap even at the highest compressions), this volume fraction can be related locally to the gap at a radial distance r from the point of closest approach of the two surfaces (see Figure 1):

$$\phi(r) = 2\Gamma/D(r) \tag{6}$$

Here, Γ is the adsorbed amount of polymer in units of monomer volume per unit area of mica. In terms of the adsorbance Γ' obtained from the force profiles in the previous section, $\Gamma = \Gamma'/\rho$, where ρ is the polymer density. For the geometry of a sphere approaching a flat surface, the gap $D(r)$ depends on the radial coordinate r according to

$$D(r) = D + r^2/2R \tag{7}$$

When the above conditions are met, the solvent flow through the polymer layer can be modeled by the Brinkman equation,[49] commonly employed in the treatment of creeping flow through porous media:

$$\eta_0\nabla^2 v - \eta_0\xi^{-2}v - \nabla P = 0 \tag{8}$$

In this equation, v is the solvent velocity field, P is the pressure, and ξ is the hydrodynamic screening length.[50,51] Physically, ξ is the length scale on which a localized solvent velocity disturbance in the polymer layer decays due to multiple scattering from the polymer segments. Like the static correlation length in a semidilute polymer solution,[48]

ξ is approximately independent of polymer molecular weight and scales in the semidilute regime ($\phi \ll 1$) of moderately overlapping layers as

$$\xi = \text{const} \times a\phi^{-\alpha} \tag{9}$$

where a is a length comparable to the monomer size[52] and α is a positive scaling exponent. Although there remains some uncertainty in the values of α,[51,53-55] it is generally believed that, in the asymptotic semidilute regime, α takes the value 3/4 in good solvents and the value 1 in Θ solvents. Since the volume fraction is a function of the radial coordinate r as specified above, an important feature of the Brinkman equation in the present application is that the frictional coupling between solvent and polymer, described by the coefficient $\eta_0\xi^{-2}$, diminishes with increasing r. We also note that eq 8 is a coarse-grained description of momentum conservation valid only for length scales exceeding ξ. This imposes a lower bound on the range of applicability of the theory, i.e., $\xi \ll D \ll 2L$.

Fredrickson and Pincus[32] solved the Brinkman equation given above for steady compression of a sphere of radius R against a flat surface in the lubrication limit, $D/R \ll 1$. They assumed asymptotic semidilute conditions for which the solvent velocity field can be taken to be divergence-free and for which the screening length has a power law dependence on concentration. By integrating the pressure fields over the lower surface, they obtained the following modified Reynolds formula for the lubrication force:

$$F_H = (4/3)\pi R^2\eta_0(\dot{D}/D)(D/\xi)^2 \tag{10}$$

where $\xi = \xi(D)$ is the value of the hydrodynamic screening length at $r = 0$. Note that only the constant coefficient 4/3 in this expression depends on the value taken for α. If we use this force expression to interpret low-frequency dynamic experiments, the analog of eq 4 for overlapping polymer layers can be written

$$\mathcal{G} = D/\eta_{\text{eff}} \tag{11}$$

with an effective viscosity given by

$$\eta_{\text{eff}} = (2/9)(D/\xi)^2\eta_0 \tag{12}$$

By combining this result with eqs 6 and 9, it follows that the effective viscosity of the polymer layer is generally D-dependent and scales as

$$\eta_{\text{eff}} \sim \eta_0 a^{-2}\Gamma^{2\alpha}D^{2(1-\alpha)} \tag{13}$$

For the asymptotic semidilute regime in good solvents ($\alpha = 3/4$), this would imply the scaling $\eta_{\text{eff}} \sim \eta_0 a^{-2}\Gamma^{3/2}D^{1/2}$. We should also note that it has been proposed[54] that the good solvent scaling exponent holds strictly for the case of $\phi \ll 1$ and that the Θ solvent scaling behavior ($\alpha = 1$) is rapidly approached on increasing ϕ, even in good solvents. Neutron spin–echo experiments[55] seem to confirm this proposition.

We come finally to consider the predictions summarized above (eqs 11–13) in relation to the present experiments. Curves corresponding to eq 11 with values of the exponent $\alpha = 1$ and 3/4 (eq 13) are shown in Figure 7. Since the value of the adsorbance Γ is known from the experimentally determined surface excess Γ', there are no adjustable parameters in this fit; the undetermined constant prefactor in eq 9 is expected to be of order unity and can in any case be estimated directly by comparison with scattering experiments.[55] The validity of the treatment leading to eqs 11–13 is limited to $D \ll 2L$, and we choose to limit the calculated curves in Figure 7 to the range $D < {}^1/_3(2L)$. As expected and as also seen from Figure 6, for $D > 2L$ we have the limiting behavior given by eq 5; presumably, there is an (unknown) interpolation relation connecting the two regimes.

As seen in Figure 7, the curve corresponding to $\alpha = 0.75$ is clearly much closer to the data than that corresponding to $\alpha = 1$. This indicates strongly that—within the validity of the theoretical treatment—the hydrodynamic screening length ξ within the brush varies with polymer concentration in accord with the expectations of scaling theory rather than with the mean-field relation (for which $\alpha = 1$). This is a gratifying observation, as direct indications for the variation of ξ in semidilute polymer solutions are difficult to obtain experimentally; even the most systematic attack on the problem, via small-angle neutron scattering,[55] could not discriminate incisively between the two exponents.[56] We note that the mean volume fraction of polymer in the polymer brushes, given by $\phi(D) = 2\Gamma/D$, is in the range $\phi \approx 0.03$–0.12 over the range of 2200 Å ($=2L$) $< D <$ 500 Å, which is where all the data for compressed brushes were taken. These ϕ values are well within the range of semidilute concentrations where the scaling exponent $\alpha = {}^3/_4$ might be expected to hold.[48,55]

A noteworthy feature of Figure 7 is that the data do not approach the $\mathcal{G} = 0$, $D = 0$ limit smoothly as predicted by eqs 11–13; rather, the slope of the $\mathcal{G}(D)$ plot in the range $D \leq 1000$ Å is considerably higher than predicted, and if the trend of the data were extrapolated, they would appear to intercept the surface separation axis at $D = D_0 \approx 400$ Å. From the definition of $\mathcal{G}$, it is as though the polymer brushes became solid-like (i.e., $A \to 0$ in the dynamic experiments) on compression to a surface separation D_0. One obvious contribution to this is the finite volume of the surface-attached chains and the fact that in toluene at room temperature polystyrene solutions become glassy—i.e., the long-ranged molecular relaxations become frozen out—at a concentration of some 85% polymer.[57] For the present adsorbance value of some 3 mg of polymer per surface, this concentration is only reached when the surface separation D is around 80 Å. It is then of interest to consider the reasons why the relaxations of the chains in the compressed brushes become extremely long—so that the brush appears rigid at short times—already at much lower volume fractions. In the present geometry the chains are attached to the mica surfaces and, in addition, confined by them to a narrow gap; as a result, their long-ranged mobility is much reduced.

At high compressions of the brushes the end-tethered polymer chains become substantially entangled: this implies that long-ranged relaxations need to take place by a "chain-retraction" mechanism[58] much as has been proposed for the arms of entangled star polymers. The time for such relaxation processes then increases exponentially with the length of the end-tethered N-mer chains. We may write the time τ_{teth} for these longest relaxations (by chain retraction) as[48]

$$\tau_{\text{teth}}(N,\phi) \approx \tau_{\text{free}}(N,\phi)\ \exp(\text{const} \times N/g) \tag{14}$$

where τ_{free} is the longest relaxation time for the chains when in a bulk, entangled semidilute solution at the same mean volume fraction ϕ as in the compressed brush; here g is the number of monomers in a correlation length (blob) of the semidilute solution, related to the volume fraction as[48] $g = a\phi^{-5/4}$. The longest relaxations of entangled free (i.e., untethered) chains proceed by reptation, for which the time in semidilute solutions is given by[48]

$$\tau_{\text{free}} = \text{const} \times (\eta_0 a^3/k_BT)N^3\phi^{3/2} \tag{15}$$

Thus compression of the brushes, leading to an increase

in the mean volume fraction ϕ in accordance with eq 6, increases the relaxation times of the chains comprising the brushes as

$$\tau_{teth}(N,\phi) \sim D^{-3/2} \exp(\text{const} \times N(D/2\Gamma)^{-5/4}) \quad (16)$$

Clearly, the exponential in eq 16 can rapidly lead to extreme slowing down of the chain relaxations at low D values and thus to an elastic (solid-like) behavior of the compressed brush layers at sufficiently short times, i.e., high values of the frequency ω of the applied motion (an effect not considered in the theoretical treatment of the lubrication forces leading to the prediction of eqs 11–13). We note that while in principle we could try to obtain a quantitative estimate for the magnitude of this effect, in practice the value of the constant in the exponential in eqs 14 and 16 is not well known for semidilute solutions.[59] In practice such a solid-like behavior implies that, at the characteristic oscillation frequencies ω of the top surface, the bottom surface responds elastically, so that A (eq 3) and hence $\mathcal{G}$ (eq 4) go to zero. We recall that in *quasistatic* measurements of the equilibrium force profile $F(D)$, as in Figure 5 (and especially the data of ref 33, also summarized as the curve in Figure 5), there is no indication of solid-like layers at $D < \sim 400$ Å, in line with the idea that such behavior is observed only at finite compression rates (sufficiently high ω values).

Finally, we remark that similar effects have been observed for polystyrene brushes in toluene when sheared under high compressions:[60] a solid-like response of the chains was indicated at monomer concentrations within the brush that were much lower than the corresponding bulk concentration for the glass transition.

To summarize: the lubrication forces acting normally between two polymer-brush-bearing mica surfaces in a good solvent medium as the surface separation D is varied sinusoidally in time may be considered to exhibit two regimes. For $D > 2L$ (where L is the effective brush thickness deduced from the onset of repulsion in the quasistatic force–distance profiles), the hydrodynamic forces between the surfaces are characteristic of the bulk viscosity of the solvent, with a shear plane shifted to a distance L_H from each mica surface. Within the range of our experimental parameters, we find $L \approx L_H$, suggesting a rather weak penetration of the fluid flow field into each brush. For $D < 2L$ (i.e., compressed brushes), fluid flow within the intersurface gap is characterized by an "effective viscosity" which varies with D in semiquantitative accord with a recent theoretical model, with a hydrodynamic screening length within the brush layers which varies in agreement with scaling rather than mean-field expectations. However, as the brush layers are progressively more strongly compressed, the response of the confined polymer chains appears to become solid-like; this occurs at monomer concentrations within the gap that are substantially lower than the glass transition composition of the bulk polymer solution at the same temperature. This behavior suggests that the confinement and attachment of the chains to the surfaces considerably increases their relaxation times, in accord with recent studies on the shear of confined polymer brushes. Experiments to explore the relation between normal and lateral lubrication forces between surfaces bearing polymer layers are currently in progress.

Acknowledgment. We thank Tom Witten for useful suggestions. We thank B.P. (America) (J.K. and P.P.), the DOE (Grant DE-FG03-87ER45331) (Y.K., H.Y., J.N.I., G.H.F., and P.P.), and the Ministry of Science (Israel) (J.K.). for support of this work. Y.K. also thanks Fuji Film Co. G.H.F. is grateful to the National Science Foundation for support under PYI Grant DMR-9057147.

References and Notes

(1) Vincent, B. *Adv. Colloid Interface Sci* **1974**, *4*, 193.
(2) Goodwin, J., Ed. *Colloidal Dispersions*; Royal Society of Chemistry: London, 1982.
(3) Pincus, P. In *Lectures on Thermodynamics and Statistical Mechanics*; Gonzales, A. E., Varea, C., Eds.; World Scientific: Singapore, 1989; p 74.
(4) de Gennes, P. G. *Adv. Colloid Interface Sci.* **1987**, *27*, 189.
(5) Alexander, S. *J. Phys. (Fr.)* **1977**, *38*, 983.
(6) Scheutjens, J. H. M.; Fleer, G. *Macromolecules* **1985**, *18*, 1882.
(7) Klein, J. In *Les Houches Session XLVIII 1988—Liquids at Interfaces*; Charvolin, J. F., Joanny, J.-F., Zinn-Justin, J., Eds.; Elsevier: Amsterdam, 1990; p 239.
(8) Patel, S.; Tirrell, M. *Annu. Rev. Phys. Chem.* **1989**, *40*, 597.
(9) Klein, J. *Macromol. Rev.* **1992**, *A29*, 99.
(10) Klein, J. *Pure Appl. Chem.* **1992**, *64 (11)*, 1577.
(11) See: Colloidal Dispersions. *Discuss. Faraday Soc.* **1990**, *90*.
(12) Happel, J.; Brenner, H. In *Hydrodynamics at Low Reynolds Numbers*; Prentice-Hall: Englewood Cliffs, NJ, 1965.
(13) Tabor, D. In *Friction*; Doubleday: New York, 1973.
(14) Lee, L.-H., Ed. *New Trends in Physics and Physical Chemistry of Polymers*; Plenum Press: New York, 1989.
(15) See: *Polymer Adsorption and Dispersion Stability*; Goddard, E. D., Vincent, B., Eds.; ACS Symposium Series 240; American Chemical Society: Washington, DC, 1984.
(16) See, e.g., ref 12, p 322.
(17) Reynolds, O. *Philos. Trans. R. Soc. London* **1886**, *177*, 157.
(18) Klein, J. *J. Chem. Soc., Faraday Trans. 1* **1983**, *79*, 99.
(19) Israelachvili, J. N.; Tirrell, M.; Klein, J.; Almog, Y. *Macromolecules* **1984**, *17*, 204.
(20) Israelachvili, J. N.; Adams, G. A. *J. Chem. Soc., Faraday Trans. 1* **1978**, *74*, 974.
(21) Chan, D. Y. C.; Horn, R. *J. Chem. Phys.* **1985**, *83*, 5311.
(22) Israelachvili, J. N. *J. Colloid Interface Sci.* **1986**, *110*, 263.
(23) Christenson, H. K.; Israelachvili, J. N. *J. Colloid Interface Sci.* **1987**, *119*, 194.
(24) Israelachvili, J. N.; Kott, S. J.; Fetters, L. J. *J. Polym. Sci. Polym. Phys. Ed.* **1989**, *27*, 489.
(25) Montfort, J. P.; Hadziioannou, G. *J. Chem. Phys.* **1988**, *88*, 7187.
(26) Van Alsten, J.; Granick, S. *Macromolecules* **1990**, *23*, 4856.
(27) Israelachvili, J. N. *Colloid Polym. Sci.* **1986**, *264*, 1060.
(28) Klein, J.; Perahia, D.; Warburg, S. *Nature* **1991**, *352*, 143.
(29) Yoshizawa, H.; Chen, Y. L.; Israelachvili, J. N., submitted.
(30) Horn, R.; Israelachvili, J. N. *Macromolecules* **1988**, *21*, 2836.
(31) Equation 4 applies[22] only in the limtis $K \gg dF/dD$, $A \ll D$, inequalities which are both well approximated in the conditions of our experiments.
(32) Fredrickson, G.; Pincus, P. *Langmuir* **1991**, *7*, 786.
(33) Taunton, H. J.; Toprakcioglu, C.; Fetters, L. J.; Klein, J. *Macromolecules* **1990**, *23*, 571.
(34) Luckham, P. F.; Klein, J. *J. Chem. Soc., Faraday Trans. 1* **1990**, *86*, 1363.
(35) To improve the accuracy of the dynamic measurements, which require a plot of $\mathcal{G}$ against D (eq 4), values of $0.9 \geq (A_0 - A)/A_0 \geq 0.2$ were generally sought. This required higher driving frequencies $\omega/2\pi$ (1 Hz) and weaker K values (ca. 10^2 nN/nm) in the absence of surface-attached polymer layers or at surface separations $D > 2L$ for the case of brush-covered surfaces (brush thickness L), while lower driving frequencies ($\omega/2\pi$ down to 0.1 Hz), larger driving amplitudes (A_0 up to 3000 Å), and a stiffer lower spring ($K \approx 10^3$ nN/nm) were used at strong compressions ($D \ll 2L$).
(36) Luckham, P. F.; Klein, J. *Macromolecules* **1985**, *18*, 721.
(37) Taunton, H. J.; Toprakcioglu, C.; Fetters, L. J.; Klein, J. *Nature* **1988**, *332*, 712.
(38) Possible systematic uncertainties in the precise values of the spring constant K and in the value of R may be adjusted at this stage, if necessary, by comparing with the known value of the solvent viscosity.
(39) *Handbook of Chemistry and Physics*, 54th ed.; CRC Press: Cleveland, 1973.
(40) A weak short-range repulsion in the surface separation range $150 < D < 20$ Å (Figure 2, crosses) suggests some loose surface attachment of PS may be occurring; the polymer detaches on slight compression, which brings the surfaces into strong adhesive contact as in the polymer-free solvent.

(41) This may reflect the presence of the loosely-attached PS layer.[40]
(42) Barrat, J.-L. *Macromolecules* **1992**, *25*, 832.
(43) Milner, S. *Macromolecules* **1991**, *24*, 3704.
(44) This prediction is based on the assumption of a parabolic segment density distribution within the brush, as obtained from self-consistent-field calculations.[46,47] Assumption of a uniform segment distribution leads to a much weaker penetration $l_p \approx \xi$.
(45) Klein, J.; Luckham, P. F. *Macromolecules* **1986**, *19*, 2007.
(46) Milner, S. T.; Witten, T. A.; Cates, M. E. *Macromolecules* **1988**, *21*, 2610.
(47) Zhulina, E. B.; Priamitsyn, V. A.; Borisov, O. V. *Vysokomol. Soedin. Ser. A* **1989**, *30*, 1615.
(48) de Gennes, P.-G. In *Scaling Concepts in Polymer Physics*; Cornell University Press: Ithaca, NY, 1975.
(49) Brinkman, H. C. *Appl. Sci. Res.* **1947**, *A1*, 27.
(50) Doi, M.; Edwards, S. F. In *The Theory of Polymer Dynamics*; Oxford University Press: New York, 1986.
(51) de Gennes, P.-G. *Macromolecules* **1976**, *9*, 587.
(52) Given by $a = bC_\infty^{1/2} = 6.6$ Å, where C_∞ is the characteristic ratio for polystyrene and b is the mean length of a backbone bond.
(53) Edwards, S. F.; Muthukumar, M. *Macromolecules* **1984**, *17*, 586.
(54) Muthukumar, M.; Edwards, S. F. *Polymer* **1982**, *23*, 345.
(55) Richter, D.; Binder, K.; Ewen, B.; Stuhn, B. *J. Phys. Chem.* **1984**, *88*, 6618.
(56) We remark that, by inspection of eq 11–13, one expects $\mathcal{G}(\alpha = 1) > \mathcal{G}(\alpha = 0.75)$ whenever $D > \Gamma$ (as seen also from the curves in Figure 7), i.e., whenever D exceeds a few nanometers in our experiments. This may explain the different variation of the normalized $\mathcal{G}(D)$ profiles shown in Figure 8, where the value of $\mathcal{G}$ for the poor solvent case ($\alpha = 1$) is greater than its value for the good solvent case ($\alpha = 0.75$) over the relevant surface separation range.
(57) Mark, H.; Bikales, N., Eds.; *Encyclopedia of Polymer Science and Engineering*; Wiley: New York, 1985.
(58) A similar idea was proposed for stress relaxation in lamellar copolymer mesophases by Witten et al.: Witten, T.; Pincus, P.; Leibler, L. *Macromolecules* **1990**, *23*, 824.
(59) The relaxation time for an entangled end-tethered N-mer in the melt is given by $\tau_{teth}(N) \approx \tau N_{free}(N) \exp(\nu N/N_e)$, where N_e is the entanglement degree of polymerization and ν is a constant of order unity whose value is known (see, e.g.: Klein, J. *Macromolecules* **1986**, *19*, 105). However, it is not clear how the number of entanglement lengths maps in terms of N_e and ϕ in an entangled semidilute solution.[48]
(60) Klein, J.; Kumachova, E.; Mahalu, D.; Perahia, D.; Warburg, S., in preparation.